# Tissue segmentation improves prostate cancer detection with artificial neural networks analysis of $^1$H MRSI

**L. Matulewicz[1], J. F. Jansen[1], H. A. Vargas Alvarez[1], O. Akin[1], S. Fine[1], A. Shukla-Dave[1], J. Eastham[1], H. Hricak[1], J. A. Koutcher[1], and K. L. Zakian[1]**
[1]Memorial Sloan-Kettering Cancer Center, New York, New York, United States

**Introduction:** Visual inspection of large proton magnetic resonance spectroscopic imaging ($^1$H-MRSI) datasets of the prostate is time-consuming and requires extensive spectroscopic expertise. Therefore introduction of an automatic method of analysis could help to promote the clinical use of MRSI. The application of artificial neural networks (ANNs) for classification of spectra for various pathologies as well as for metabolite quantification has been demonstrated [1]. ANNs do not require a priori knowledge of the relationship among the variables in the problem, such as identification of the chemical compounds in the spectra. In contrast to visual analysis by spectroscopists ANNs use the complete information contained in the raw data to address a diagnostic question, in this case discrimination of malignant vs. benign voxels – directly. The goal of this study is to assess whether an ANN model is a useful tool for automatic detection of tumor voxels in the prostate from $^1$H-MRSI datasets with additional information about tissue segmentation.

**Materials and Methods:** 10 men with prostate cancer (median age, 54 years; range, 36-68 years) who underwent endorectal MRI/MRS before radical prostatectomy and who had no prior hormonal or radiation treatment were included in this study. These patients had at least one tumor on whole–mount histopathological map and at least one suspicious MRSI voxel detected (as defined below). 3D $^1$H-MRSI examinations were performed on a 1.5-T whole-body unit (Signa Horizon; GE Medical Systems) with an endorectal coil (Medrad, Pittsburgh, PA) and PROSE acquisition package (GE Medical Systems) in a location prescribed by T2-weighted fast spin-echo images (4400/(effective) 102; echo train length, 12; section thickness, 3 mm; intersection gap, 0 mm; field of view, 14 cm; matrix, 256x192). The spectroscopic acquisition parameters were as follows: PRESS voxel selection, 1000/130 ms [TR/TE]; one average; spectral width, 1250 Hz; number of points, 512; field of view, 11 x 5.5 x 5.5 cm$^3$; and 16 x 8 x 8 phase encoding steps. Spectral data were automatically processed by Functool software (GE Medical Systems). The data in GE format within the range 4.3 - 0.4 ppm (256 points) were used and real spectra were exported for future analysis. In each patient, all voxels within the PRESS excitation volume were labeled as healthy or suspicious by an experienced spectroscopist according to established decision rules based on the resonances of total choline (Cho) at 3.2 ppm, creatine/phosphocreatine (Cr) at 3.0 ppm, polyamines (PA) at 3.1 ppm and citrate (Cit) at 2.6 ppm [2] (total of 2903 voxels in 10 patients). Of the 116 voxels marked as suspicious, 86 voxels were labeled as true tumor voxels based on histopathological maps and voxel locations matched with sextant precision by an experienced radiologist and an experienced pathologist (>10 yrs of experience). Tissue segmentation on MRI was performed by the radiologist who outlined the peripheral zone (PZ), transition zone (TZ) and periurethral region (U) on T2-weighted images. With this information, every MRSI voxel was assigned with a percentage of PZ, TZ, U and/or outside the gland area (O). The dataset was randomly divided into a training set (70%), validation set (15%) and test set (15%). Multilayer perceptron networks (MLP) were implemented using MATLAB's Neural Network Toolbox (Mathworks; Natick, MA) to automatically predict tumor voxels. Two different ANNs were created with different datasets used as inputs: ANN(1) with the input of spectra alone and ANN(2) with the spectra combined with tissue segmentation labels.

**Results:** Figure 1 shows mean resonance intensity values (±SD) of spectra in tumor, U, PZ or TZ. As expected, the most characteristic marker of the tumor is Cho signal (Fig. 1a); however, the same signal with similar intensity can be observed in periurethral region (Fig. 1b) which may be due to glycerophosphocholine (GPC) in seminal fluid. Tumor tissue spectra also reveal a relatively elevated unidentified compound at 2.06 ppm; however, this region is in the transition band of the spectral-spatial excitation pulses [3] and conclusions cannot be drawn without further investigation.

ANN(1) contained 256 inputs, 8 neurons in the hidden layer, and 2 outputs (corresponding to the 2 categories of the target variable *tumor* vs. *healthy*), with an overall correct classification rate at 99% (Table 1a). ANN(2) contained 260 inputs, 15 neurons in the hidden layer, and 2 outputs with an overall classification rate at 99.45% (Table 1b). The key parameter for evaluation of the method is the correctness of prediction of tumor voxels (Table 1, column "tumor"). ANN(2) with the segmentation information (Table 1b) revealed 91.9% of correctly predicted tumor voxels vs. 76.7% correctly identified by ANN(1) relying on spectra alone (Table 1a). The number of voxels identified by ANN as tumor (nine), but labeled as healthy by visual inspection, was exactly the same for both models.

**Discussion and Conclusions:** We demonstrated the ANN's accuracy for automatic detection of tumor voxels in the prostate MRSI datasets. We also showed that applying tissue segmentation from MRI as an additional input to ANN improves the accuracy of detecting tumor voxels from MRSI. The results of the ANN(2) analysis with tissue segmentation (Table 1b) showed fewer missed tumor voxels in comparison to visual analysis and ANN(1) analysis with only spectra used as inputs (Table 1a). As expected, both ANNs perform better than the visual analysis, because only true positive voxels confirmed by histopathology are used to train ANN, while this information is not available to the spectroscopist. Voxels identified by ANN as tumor, but labeled as healthy by a spectroscopist, should be localized on histopathological maps to check whether they were missed by a spectroscopist. A drawback of the current implementation is that it does not use the information about lesions that are not detected by visual assessment of MRSI. In the future, the sensitivity of cancer detection by ANN can be potentially improved by fusing MR images with histopathological maps and using the precise locations of the tumor from the maps to inform the ANN about the locations of missed tumor voxels. It is also important to increase the number of cases and to test and re-train the ANN models for the best possible generalization of the method.

**References:** 1.Bhat et al. 183(1):110. (2006); 2.Shukla-Dave et al. 245(2):499. (2007); 3.Schricker et al. 46(6):1079. (2001); *Supported by NIH grant No.R01 CA76423*

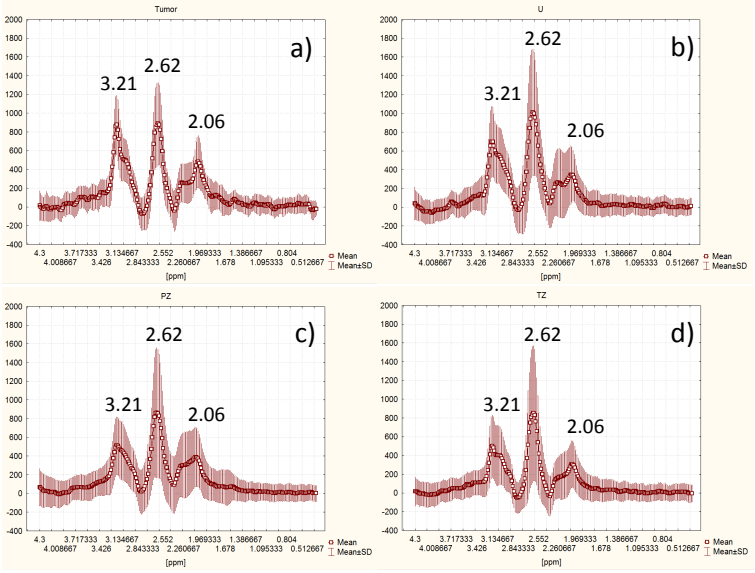


**Figure 1.** Mean ± SD values of resonance signal intensity versus ppm positions for groups of spectra labeled as **a)** tumor (86 spectra) **b)** periurethral region U (227 spectra) **c)** PZ (693 spectra) **d)** TZ (753 spectra).

**a) input: spectra only**

| identified by ANN | labeled by the visual analysis + histopathological maps: healthy | tumor | all |
|---|---|---|---|
| Total | 2817 | 86 | 2903 |
| Correct | 2808 | 66 | 2874 |
| Incorrect | 9 | 20 | 29 |
| Correct (%) | 99.68 | 76.74 | 99.00 |
| Incorrect (%) | 0.32 | 23.26 | 1.00 |

**b) input: spectra + tissue segmentation**

| identified by ANN | labeled by the visual analysis + histopathological maps: healthy | tumor | all |
|---|---|---|---|
| Total | 2817 | 86 | 2903 |
| Correct | 2808 | 79 | 2887 |
| Incorrect | 9 | 7 | 16 |
| Correct (%) | 99.68 | 91.86 | 99.45 |
| Incorrect (%) | 0.32 | 8.14 | 0.55 |

**Table 1.** Classification of spectra by ANN with the inputs of **a)** spectra only (256 variables) **b)** spectra + tissue segmentation labels (260 variables). Columns contain voxels labeled by the visual analysis plus histopathological maps. Rows show the numbers and percentages of voxels identified by ANNs.